Journal of Materials Chemistry C

ROYAL SOCIETY OF CHEMISTRY

PAPER

View Article Online
View Journal | View Issue

Check for updates

Cite this: J. Mater. Chem. C, 2023, 11, 6981

Highly efficient near-infrared thermally activated delayed fluorescence organic light-emitting diodes with emission beyond 800 nm†

Jing-Xing Liang, ‡[a] Yukun Tang, ‡[b] Xiaofei Wang,‡[c] Kai Zhang, [c] Yu-wei Shih,[b] Chia-Hsun Chen, [d] Tien-Lung Chiu, [e] Pei Jin Li,[f] Jiun-Haw Lee, [f] Chuan-Kui Wang,*[c] Chung-Chih Wu *[b] and Jian Fan *[ag]

Received 13th February 2023,
Accepted 28th March 2023

DOI: 10.1039/d3tc00524k

rsc.li/materials-c

Near-infrared (NIR) emitters are employed in a wide range of applications such as bio-sensors, optical communication devices, and organic light-emitting diodes (OLEDs). The development of NIR thermally activated delayed-fluorescence (TADF) materials lags significantly behind that of platinum complexes and quantum dots. To achieve cost reduction and environmental sustainability, TADF OLEDs have attracted extensive attention in both the academic community and industry in recent years. Herein, a conjugated planar acceptor was applied in a TADF emitter (TCN-TPA) to enhance the intermolecular through-space electronic coupling and redshift the emission spectra at high doping levels. In addition, multiple sub-acceptor units were integrated into a rigid acceptor to narrow the band gap. Importantly, the overall robust configuration of the TCN-TPA molecule led to high photoluminescence quantum yield (PLQY). Consequently, TCN-TPA demonstrated a record-high external quantum efficiency (EQE) of 2.4% at 802 nm and 1.1% at 841 nm among TADF OLEDs in this spectral range.

Published on 30 kovo 2023. Downloaded on 2024-08-10 18:25:00.

Introduction

In recent years, there has been increasing interest in NIR emitters due to their advanced applications such as bioimaging, night vision displays, and so on.[1] TADF materials could utilize both excited singlet (S_1) and triplet (T_1) states and realize 100% internal quantum efficiency theoretically.[2] Therefore, TADF materials were considered as an important class of emitting materials for achieving efficient NIR OLEDs.[3,4] Thanks to the various synthetic routes to the functionalization of targeted molecules, a great number of TADF materials with different chemical, physical, and optical properties have been prepared. Compared to blue, green, and red TADFs, NIR TADFs with an emission of over 700 nm have been much less investigated.[5–8] In 2015, Wang *et al.* reported a V-shaped molecule TPA-DCPP that achieved a maximum EQE of 2.1% at 710 nm with a non-doped device.[9] In 2017, Liao *et al.* introduced acenaphthene into a NIR-TADF APDC-DTPA, and the non-doped OLED demonstrated a maximum EQE of 2.19% at 777 nm.[10] Later, Qiao *et al.* reported two acenaphthene-based emitters (TPAAP and TPAAQ), which showed efficient NIR emission through the formation of *J*-aggregates.[11] It is notable that the intermolecular through-space electronic coupling effect was applied in these cases to lower the S_1 energy levels and consequently to push the emission band into the NIR region.

For conventional fluorescence materials, the strong intramolecular conjugation effect between the donor and acceptor units could effectively narrow the bandgaps and redshift the emission bands beyond 800 nm. However, there have been only a few reports on TADF OLEDs showing emission over 800 nm until now.[12–17] Meanwhile, a small S_1–T_1 energy gap (ΔE_{ST}) is generally considered as a prerequisite for constructing an efficient TADF. Therefore, the highest occupied molecular orbital (HOMO) and the lowest unoccupied molecular orbital

[a] Institute of Functional Nano & Soft Materials (FUNSOM), Jiangsu Key Laboratory for Carbon-Based Functional Materials & Devices, Soochow University, Suzhou, Jiangsu 215123, China. E-mail: jianfan@suda.edu.cn
[b] Department of Electrical Engineering, Graduate Institute of Electronics Engineering and Graduate Institute of Photonics and Optoelectronics, National Taiwan University, Taipei 10617, Taiwan. E-mail: wucc@ntu.edu.tw
[c] Shandong Province Key Laboratory of Medical Physics and Image Processing Technology, School of Physics and Electronics, Shandong Normal University, 250014 Jinan, China. E-mail: ckwang@sdnu.edu.cn
[d] Department of Chemistry, National Taiwan University, Taipei 10617, Taiwan
[e] Department of Electrical Engineering, Yuan Ze University, Taoyuan 32003, Taiwan
[f] Graduate Institute of Photonics and Optoelectronics and Department of Electrical Engineering, National Taiwan University, Taipei 10617, Taiwan
[g] State Key Laboratory of Structural Chemistry, Fujian Institute of Research on Structure of Matter, Chinese Academy of Sciences, Fuzhou, Fujian 35002, China

† Electronic supplementary information (ESI) available. See DOI: https://doi.org/10.1039/d3tc00524k

‡ These authors contributed equally to this work.

Published on 30 kovo 2023. Downloaded on 2024-08-10 18:25:00.

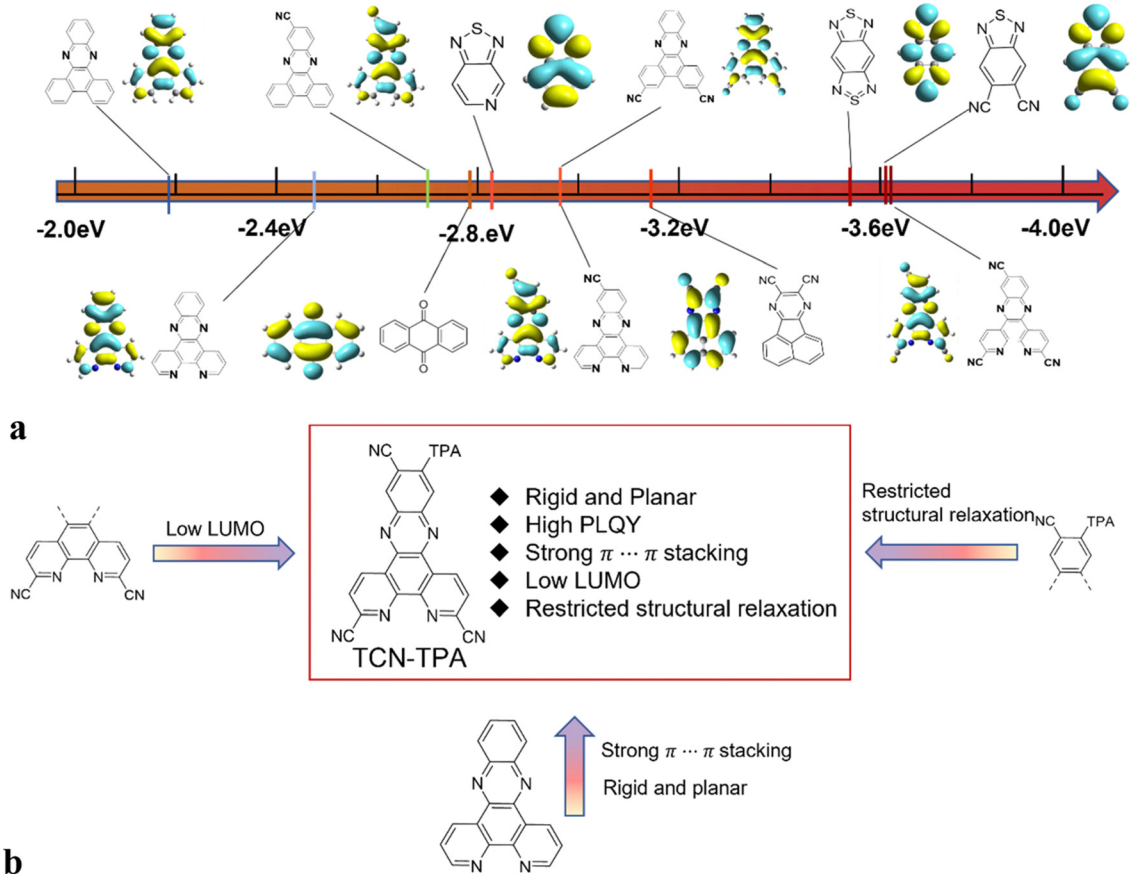

Scheme 1 (a) Comparison of the LUMO levels of various acceptors applied for TADFs and calculated with B3LYP/6-31G(d); (b) the chemical structure and molecular design strategy of TCN-TPA.

(LUMO) should be widely separated, which usually would lead to limited electronic communication between the HOMO and LUMO within the donor–acceptor (D–A) type TADFs. Considering that the HOMO and LUMO energy levels of TADFs were mainly determined by the donor and acceptor units, respectively, the introduction of strong donor and strong acceptor units into the molecular framework to enhance intramolecular charge transfer (CT) could be a straightforward method to construct a NIR TADF emitter.

In this work, we combined the intermolecular through-space electronic coupling effect and the intramolecular CT strategy to design an NIR TADF emitter (TCN-TPA) with triphenylamine (TPA) as the donor and dipyrido[3,2-*a*:2′,3′-*c*]phenazine-3,6,11-tricarbonitrile (TCN) as the acceptor. As shown in Scheme 1, the TCN unit containing three CN groups and four sp^2 hybridized N atoms is a strong electron-withdrawing motif relative to most of the reported acceptor units, giving an extremely low LUMO energy level of TCN-TPA. The planar polycyclic aromatic system of TCN resulted in an extensive intermolecular π···π interaction in thin films at high doping ratios, which shifted the emission deep into the NIR region. It is worth mentioning that NIR TADF emitters may suffer from severe non-radiative decay due to their narrow bandgaps. However, we can achieve high photoluminescence efficiency of NIR TADF *via* delicate molecular engineering. The crowded arrangement of CN and TPA in TCN-TPA restricted the vibration and rotation of the TPA unit greatly. In addition, the rigidity of TCN will also reduce the non-radiative decay to a certain degree. With a combination of these strategies, a red-shift in the EL from 756 nm to 841 nm was observed for TCN-TPA based OLEDs upon increasing the doping ratios from 9 to 50 wt%. Notably, the EQE of TCN-TPA based OLEDs reached 1.1% with the emission peak at 841 nm.

Results and discussion

The synthetic route to TCN-TPA is shown in Scheme S1 (ESI†). The condensation reaction between 4,5-diamino-4′-(bis(4-(*tert*-butyl)phenyl)amino)-4,5-dihydro-[1,1′-biphenyl]-2-carbonitrile and 2,9-dimethyl-1,10-phenanthroline-5,6-dione under acidic conditions produced pyrazine. The oxidation reaction with SeO_2 converted the methyl group into an aldehyde. The following condensation reaction with hydroxylamine gave the oxime and then the dehydration reaction yielded the target compound, which was confirmed with ^{1}H NMR spectroscopy, MALDI-TOF mass spectrometry, high resolution mass spectrometry (HRMS) and ^{13}C NMR spectroscopy (Fig. S1–S7, ESI†). The HOMO of TCN-TPA determined with cyclic voltammetry was

 This journal is © The Royal Society of Chemistry 2023

Published on 30 kovo 2023. Downloaded on 2024-08-10 18:25:00.

Table 1 Summary of the physical properties of TCN-TPA

Compound	λ_{abs}[a] (nm)	λ_{em}[a] (nm)	$PL_{fl/ph}$[b] (nm)	$\Phi_{PL,sol}$[a] (%)	$\Phi_{PL,film}$[c] (%)	$PL_{Fl,film}$[c] (nm)	T_g/T_d[d] (°C)	HOMO/LUMO[e] (eV)	E_g[f] (eV)	S_1/T_1[g] (eV)	ΔE_{ST}[h] (eV)
TCN-TPA	396/556	720	660/678	18.7	30.5/11.0/8.7/5.7	730/775/789/803	n.a./433	−5.28/−3.33	1.95	2.17/1.97	0.20

[a] Measured in toluene at 298 K. [b] Measured in toluene at 77 K. [c] Measured in CBP at 298 K with doping ratios at 9/24/30/50 wt%. [d] T_g: glass transition temperature; T_d: decomposition temperature. [e] HOMO was calculated from CV data; LUMO as calculated from the HOMO and E_g. [f] E_g was calculated from the corresponding absorption cutoff. [g] Singlet/triplet energies (S_1/T_1) were calculated from fluorescence/phosphorescence onsets. [h] $\Delta E_{ST} = S_1 - T_1$.

−5.28 eV (Fig. S8, ESI† and Table 1), which was comparable with those of TPA based TADFs.[18–21] TCN-TPA demonstrated excellent thermostability at a decomposition temperature of 433 °C due to its robust structure (Fig. S9, ESI†).

As shown in Fig. 1, TCN-TPA showed a weak CT absorption at 556 nm. Remarkably, an intensive emission peak at 720 nm was observed for TCN-TPA in toluene. So far there have been few reports on NIR TADF with native emission over 700 nm.[12–14] Therefore, the introduction of multiple electron withdrawing groups (CN, pyrazine and pyridine) into TCN-TPA could effectively redshift the emission band. TCN-TPA showed a shoulder peak at around 800 nm. The donor unit 9, 9-dimethyl-9,10-dihydroacridine is a flexible building block, which could have two possible conformations, namely, a planar form and a crooked form. Molecules constructed from this donor can thus have two corresponding conformations, and exhibited dual emission properties.[22] The rigidity of the TCN unit could exclude the possibility of two stable conformations. The long-wavelength shoulder peak of TCN-TPA in toluene could originate from the contribution of different vibrational levels in the excited state. The S_1 and T_1 energy levels estimated from fluorescence (room temperature) and phosphorescence (77 K) onsets were 2.17 eV and 1.97 eV, respectively, giving ΔE_{ST} in toluene of 0.20 eV. Interestingly, the ΔE_{ST}s values for the thin films at 9/24/30/50 wt% doping ratios were 0.083/0.112/0.103/0.103 eV (Fig. S10, ESI†), which could enable the efficient reverse intersystem crossing (RISC) process.[23] The emission band below 550 nm in the phosphorescence spectra of the doped thin-films samples could be assigned to the emission of the CBP host.[24] Compared with the ΔE_{ST} in toluene, the reduction in ΔE_{ST}s for the doped films could be due to the enhanced intermolecular interaction in the solid state.[11] The PLQYs for 9/24/30/50 wt% doped films were 30.5/11.0/8.7/5.7% with 730/775/789/803 nm emission peaks. As the doping ratio increased, the PLQYs decreased gradually due to the aggregation induced quenching effect. However, the PLQY of TCN-TPA in the 9 wt% doped thin film (30.5%) was higher than that in toluene (18.7%), which could be due to the restricted rotation and vibration in the solid state. This redshift in the emission spectra suggested the enhanced interaction between TCN-TPA molecules as the doping ratios increased.[25] The transient PL measurements of the 9/24/30/50 wt% doped thin films revealed the prompt fluorescence with lifetimes (τ_p) in the range of 3.35–12.12 ns and the delayed fluorescence with lifetimes (τ_d) in the range of 9.6–50.1 μs (Fig. 2 and Table 2). Notably, the internal conversion decay rate from S_1 to S_0 (k_{IC}, 3.87×10^7 s^{-1}–12.80×10^7 s^{-1}) was much higher than the corresponding radiative rate constant (k_r^S, 5.94×10^6 s^{-1} –17.00×10^6 s^{-1}), partially due to the small energy gap between S_1 and S_0.

The electronic structure of TCN-TPA in toluene and in CBP (50 wt%) was studied by density functional theory. The

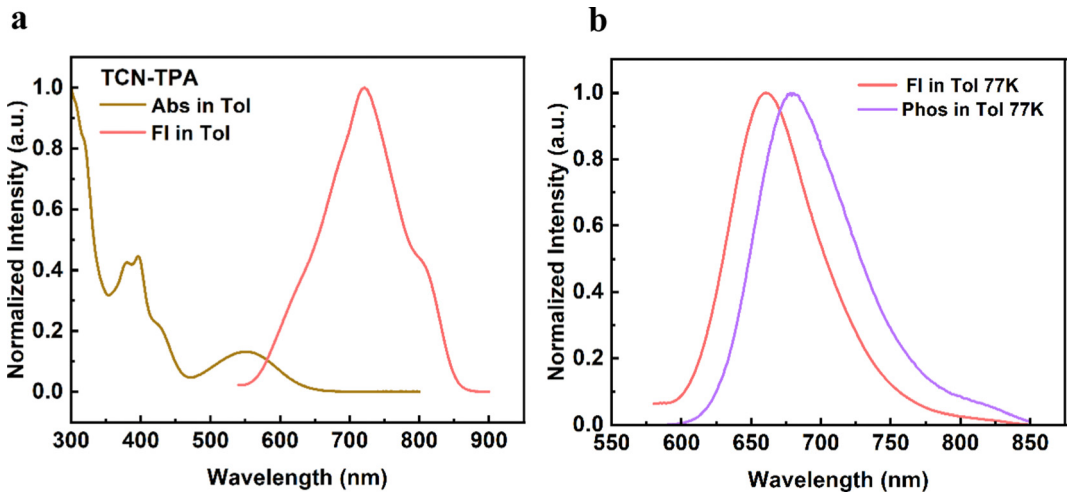

Fig. 1 Photophysical characterization of TCN-TPA. (a) Normalized UV-vis absorption and fluorescence spectra in toluene (1×10^{-5} M) at room temperature. (b) Normalized fluorescence and phosphorescence spectra in toluene (1×10^{-5} M) at 77 K.

Published on 30 kovo 2023. Downloaded on 2024-08-10 18:25:00.

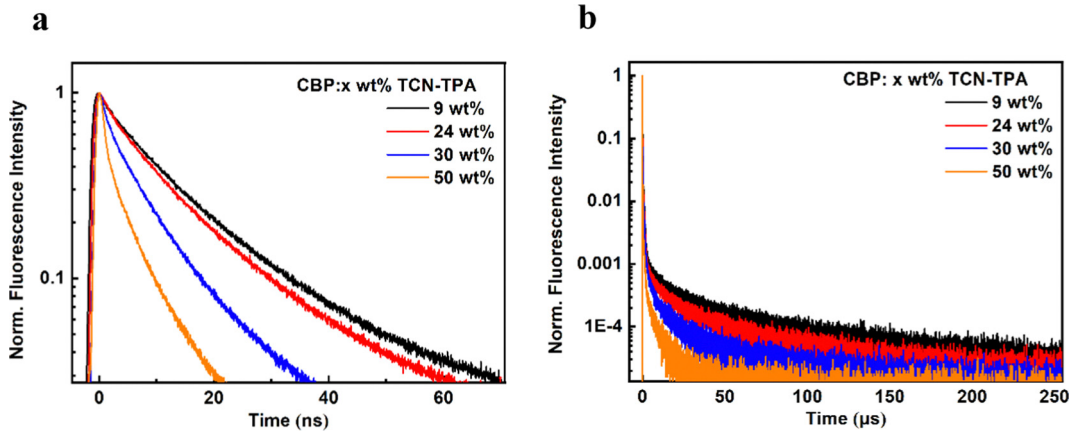

Fig. 2 (a and b) Transient PL decay curves of TCN-TPA in *x* wt% doped CBP films (*x* = 9, 24, 30, and 50).

Table 2 Photophysical characteristics of TCN-TPA doped into CBP films

Compound	Doping ratio [wt%]	Φ_{PL} [%]	Φ_p/Φ_d [%]	τ_p [ns]	τ_d [μs]	k_p [10^8 s^{-1}]	k_d [10^3 s^{-1}]	k_r^S [10^6 s^{-1}]	k_{IC} [10^7 s^{-1}]	k_{ISC} [10^7 s^{-1}]	k_{RISC} [10^3 s^{-1}]
TCN-TPA	9	30.5	9.92/20.58	12.12	50.1	0.82	6.09	17.00	3.87	2.68	9.02
	24	11.0	4.46/6.54	11.01	39.1	0.90	2.81	5.94	4.81	3.68	4.73
	30	8.7	4.10/4.59	6.65	21.2	1.50	4.10	6.91	7.25	7.08	7.76
	50	5.7	3.09/2.61	3.35	9.6	2.98	5.94	7.74	12.80	16.2	13.00

k_p is the rate constant of prompt fluorescence decay; k_d is the rate constant of delayed fluorescence decay; k_r^S is the rate constant of radiative transition from S_1 to S_0; k_{IC} is the internal conversion decay rate from S_1 to S_0; k_{ISC} is the rate constant of intersystem crossing; k_{RISC} is the rate constant of reverse intersystem crossing.

calculation details are provided in the ESI.† As expected, large dihedral angles (46.8° in toluene and 49.2° in thin films) between TPA and TCN were detected, which led to wide separation of frontier orbitals with the HOMO on TPA and

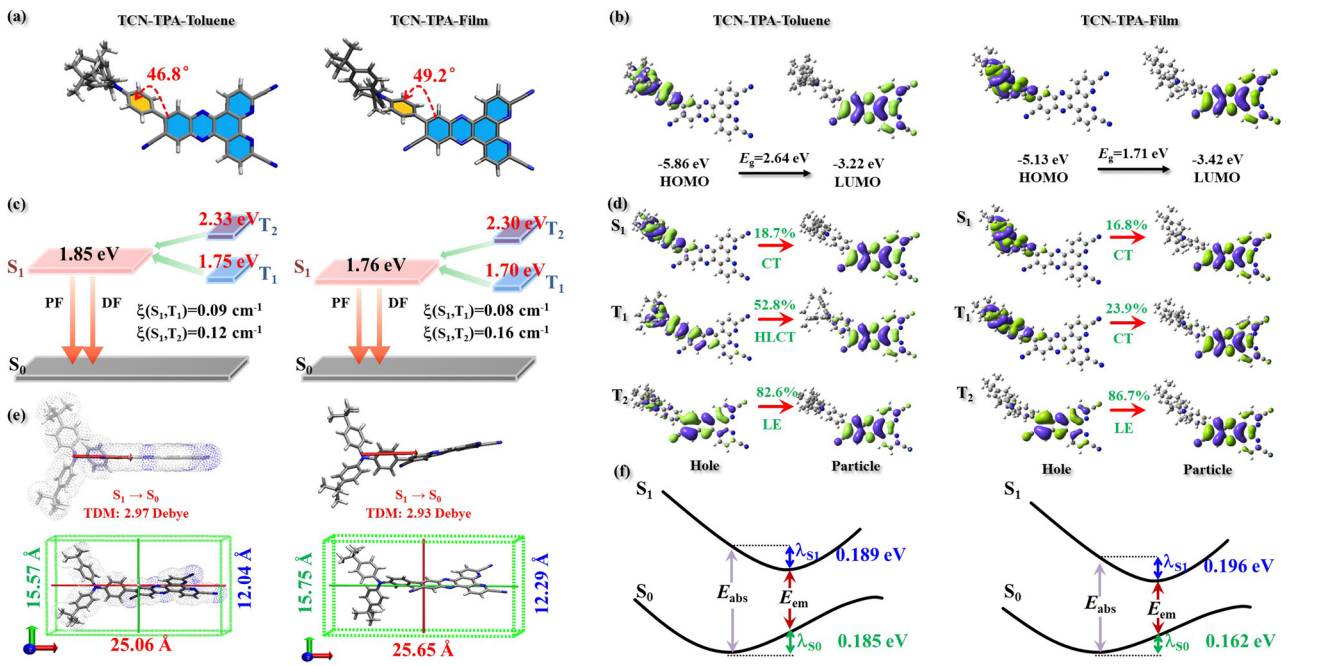

Fig. 3 (a) Molecular structure of TCN-TPA in toluene and films (50 wt% in CBP). (b) Distribution of the HOMO and LUMO. (c) The adiabatic energy diagram of the low-lying excited states and spin–orbit coupling (SOC) matrix element (ξ). (d) Natural transition orbitals (NTOs) of the low-lying excited states (The values above the arrows are the LE proportion in excitation). (e) Transition dipole moment vector contributions from the whole molecule in $S_1 \rightarrow S_0$ and the overview of the TCN-TPA molecule. (f) The relaxation energy (λ) of S_0 and S_1 states for TCN-TPA.

 This journal is © The Royal Society of Chemistry 2023

Published on 30 kovo 2023. Downloaded on 2024-08-10 18:25:00.

the LUMO on TCN (Fig. 3). The HOMO and LUMO of TCN-TPA in toluene were −5.86 eV and −3.22 eV, respectively. As shown in Fig. S11 (ESI†), TCN-TPA molecules adopted the head-to-tail (Dimer-1) and head-to-head (Dimer-2) packing patterns. Within these two types of dimers, the adjacent molecules were held together *via* π···π interaction to favor through-space electronic coupling in the doped thin film (50 wt%). As a result, TCN-TPA exhibited a narrow bandgap of 1.71 eV in the doped film with a HOMO of −5.13 eV and a LUMO of −3.42 eV. The S_1/T_1s values in toluene and in thin films were 1.85 eV/1.75 eV and 1.76 eV/1.70 eV, respectively. Therefore, the ΔE_{ST} in thin films (0.06 eV) was smaller than that in toluene (0.10 eV), which agreed well with the experimental result. Natural transition orbitals revealed a dominant CT character of S_1 (LE contribution of 18.7%) and a hybridized local and charge transfer (HLCT)[26] excited state of T_1 (LE contribution of 52.8%) for TCN-TPA in toluene. In the doped films, the S_1 and T_1 of TCN-TPA are basically CT states with LE proportions of 16.8% and 23.9%, respectively. Due to the different transition characteristics of S_1 and T_1 in toluene, TCN-TPA demonstrated a larger spin–orbit coupling (SOC) matrix element ($\xi(S_1,T_1)$ = 0.09 cm^{-1}) in toluene than in thin films ($\xi(S_1,T_1)$ = 0.08 cm^{-1}). Since there was a big energy difference between S_1 and T_2, the T_2 state could make an insignificant contribution during the RISC process though large $\xi(S_1,T_2)$s were achieved in toluene and in thin films. TCN-TPA showed a larger reorganization energy (estimated from the sum of λ_{S1} and λ_{S0}) in toluene than in doped films due to the restricted structural relaxation in the solid state. The emission wavelengths in toluene and in 50 wt% doped films were calculated to be 745 nm and 800 nm, respectively.

The side view of optimized geometry of the TCN-TPA molecule is shown in Fig. 3e, and the aspect ratios of TCN-TPA in toluene and in the solid state were 2.08 and 2.09, respectively. Thus, TCN-TPA can be considered as a rigid and linear molecule, which could enhance the horizontal emitting dipole ratio ($\Theta_{\parallel}$) and the optical out-coupling efficiency (Φ_{out}).[27] The angle-resolved *p*-polarized PL intensity measurements indicated a high $\Theta_{\parallel}$ of 80% for all the 9/24/30/50 wt% TCN-TPA doped films (Fig. 4). To study the electroluminescence (EL) performance of TCN-TPA, the devices were fabricated with the following configuration: sITO(115 nm)/MoO_3(1 nm)/di-[4-(*N*,*N*-ditolyl-amino)-phenyl]-cyclohexane TAPC (*x* nm)/4,4′-bis(carbazol-9-yl)biphenyl CBP: TCN-TPA(20 nm)/4,6-bis(3,5-di(pyridin-3-yl)phenyl)-2-methylpyrimidine B3PYMBM(*y* nm)/LiF(1 nm)/Al, with *x* = 85 nm (S1), 105 nm (S2), 125 nm (S3) and *y* = 75 nm for 9 wt% doped devices; *x* = 95 nm (S4), 115 nm (S5), 135 nm (S6)

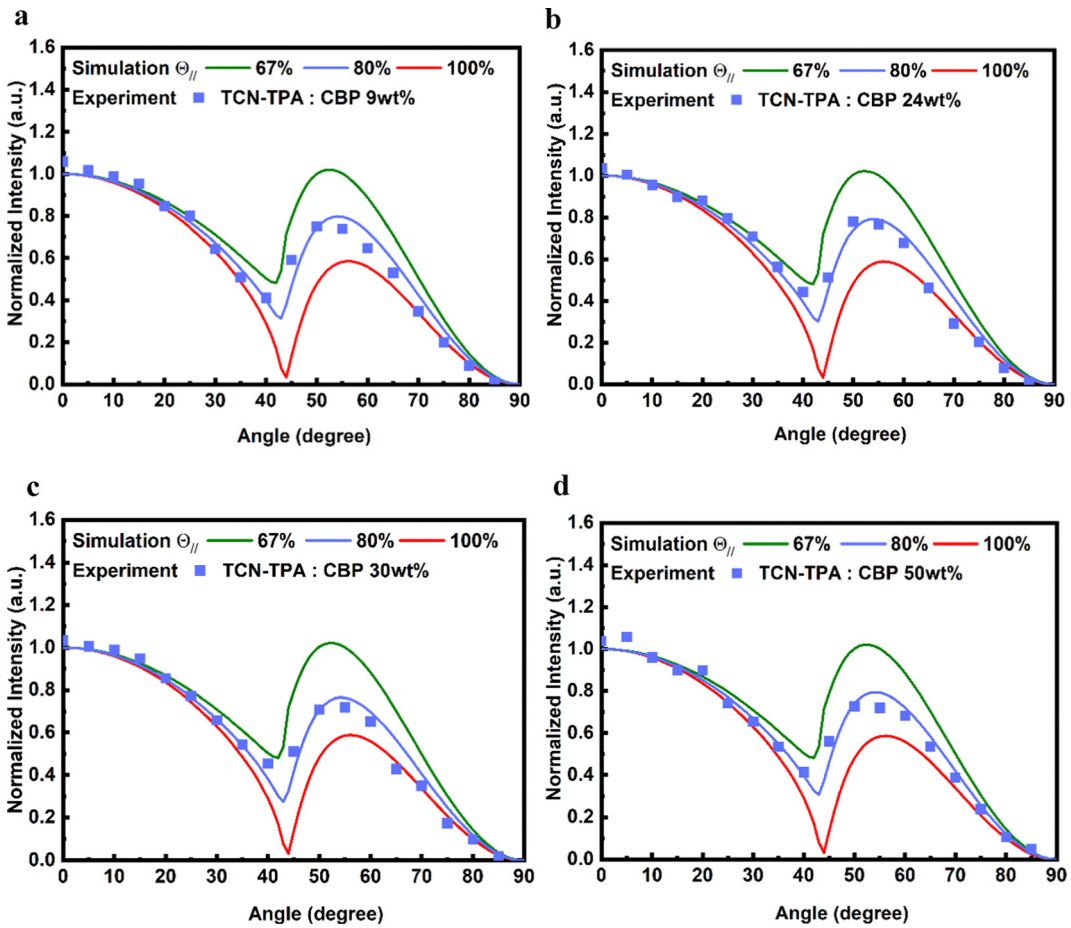

Fig. 4 (a–d) The measured angle-resolved *p*-polarized PL intensity (at PL peak wavelength) of TCN-TPA doped in the CBP host with different doping concentrations (a: 9 wt%; b: 24 wt%; c: 30 wt%; d: 50 wt%) as a function of the emission angle, along with simulated curves (line and dotted line).

Published on 30 kovo 2023. Downloaded on 2024-08-10 18:25:00.

and y = 80 nm for 24 wt% doped devices; x = 100 nm (S7), 120 nm (S8), 140 nm (S9) y = 80 nm for 30 wt% doped devices; x = 115 nm (S10), 135 nm (S11), 155 nm (S12) y = 90 nm for 50 wt% doped devices. The device structure, energy levels and molecular structures of functional layer materials are shown in Fig. S12 (ESI†). The device data are summarized in Table S1 (ESI†).

The EL properties of TCN-TPA are illustrated in Fig. 5. As the doping ratio increased, the EL peak varied in a wide range from 756 nm to 841 nm. Compared with the PL spectra, a redshift was observed in the EL spectra at a given doping ratio, which was ascribed to the microcavity effect of the device.[28] The turn-on voltage with current density exceeding 10^{-5} mA cm^{-2} decreased gradually from 2.2 V to 1.8 V with the increase in the doping ratio from 9 wt% to 50 wt%. Lee and coworkers reported that the high doping ratio of TADF emitters could result in enhanced and balanced carrier transport in the emitting layer.[29] The decrease in the turn-on voltage for TCN-TPA-based devices at the high doping ratios thus could be due to the reduced energy barrier during the charge injection and transport process. TCN-TPA demonstrated superior device performance with EQEs of 6.4/3.2/2.4/1.1% at 758/784/802/841 nm EL peaks. In addition to the high PLQY, the high Φ_{out} and exciton utilization efficiency also accounted for the state-of-the-art EL performance beyond 800 nm (Fig. 6). As shown in Table S2 (ESI†), the TADFs with EL emission over 800 nm used the TPA unit as the donor and the rigid and planar electron-withdrawing unit as the acceptor. These planar acceptor units could favor the intermolecular π···π interaction at higher doping ratios, thus red-shifting the emission wavelength. The $\Theta_{||}$, refractive index (n) and extinction coefficient (k) of each functional layer material in our devices were used for calculating Φ_{out}.[30] Assuming that the charge recombination

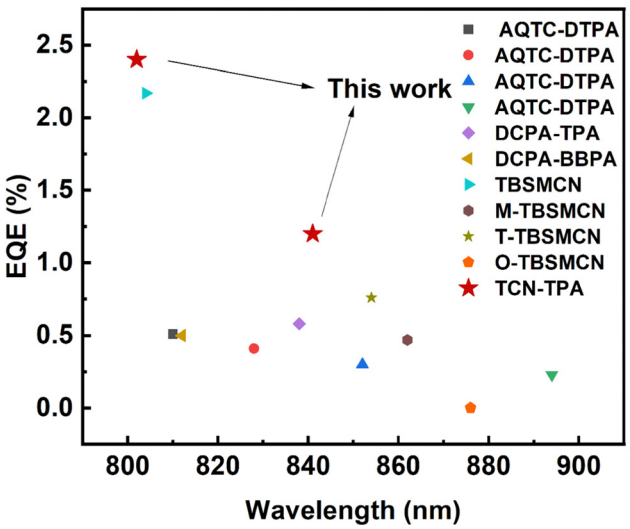

Fig. 6 Reported maximum external quantum efficiencies for TADF OLEDs with EL peaks in the range of 800–900 nm.

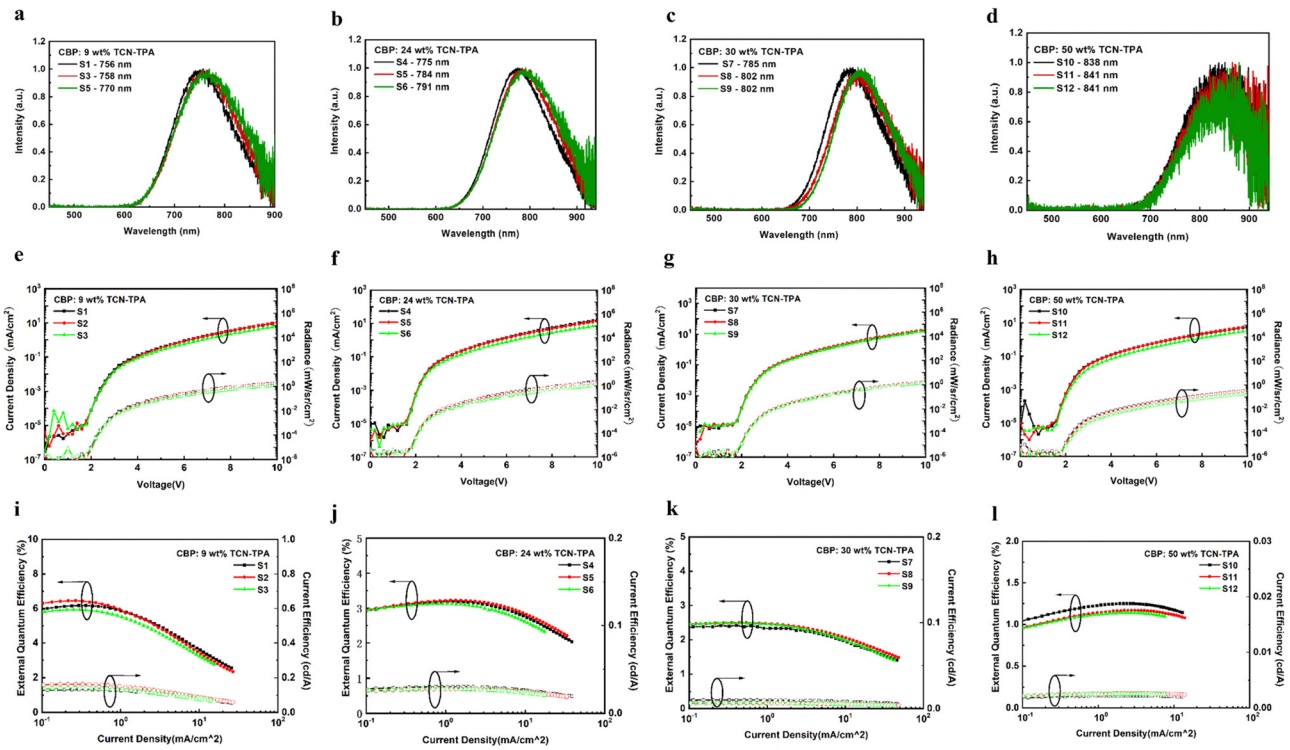

Fig. 5 (a–d) EL performance of TCN-TPA in the CBP host with 9 wt%, 24 wt%, 30 wt% and 50 wt%, respectively. Different thicknesses of TAPC were applied in devices S1–S12 (S1 = 85 nm; S2 = 105 nm; S3 = 125 nm; S4 = 95 nm; S5 = 115 nm; S6 = 135 nm; S7 = 100 nm; S8 = 120 nm; S9 = 140 nm; S10 = 115 nm; S11 = 135 nm; S12 = 155 nm). (e–h) Current density–voltage–radiance of the devices. (i–l) External quantum efficiency and current density characteristics of the devices as a function of the current density.

 This journal is © The Royal Society of Chemistry 2023

Published on 30 kovo 2023. Downloaded on 2024-08-10 18:25:00.

efficiency was 100%,[31] the Φ_{out}s and exciton utilization efficiencies were 34.8/35.8/34.2/33.7% and 62.0/84.2/83.6/71.0% (Table S3, ESI†), respectively, for the devices at the doping ratios of 9/24/30/50 wt%. The decrease in EQE at high brightness was due to the accumulation of T_1 excitons and the consequent T_1-associated quenching process in the emitting layer.

Conclusion

In summary, a NIR TADF emitter, TCN-TPA, was designed and prepared. The multiple sub-acceptor (CN group, pyrazine, and pyridine) strategy lowered the LUMO of TCN-TPA significantly and enabled the native emission in toluene over 700 nm. With the help of the strong intramolecular CT and intermolecular through-space coupling, the emission peak of TCN-TPA in doped thin films was pushed deep into the NIR region (over 800 nm). The rigid and linear configuration of TCN-TPA led to the high $\Theta_{\parallel}$(80%) and Φ_{out} (>33%). Thanks to the robust structure of TCN-TPA, the highly doped thin films with small ΔE_{ST}s (<0.12 eV) demonstrated high PLQYs (5.7–30.5%). As a result, TCN-TPA showed unprecedented EQEs of 2.4% at 802 nm and 1.1% at 841 nm.

Author contributions

C. K. W., C. C. W. and J. F. conceived the original idea and secured funding. T. L. C., J. H. L., C. K. W., C. C. W. and J. F. supervised the project and drafted the manuscript. J. X. L., Y. T., Y.-w. S., C. H. C. and P. J. L. carried out the experiment, performed the data analysis and drafted the manuscript. X. W., K. Z. and C. K. W. performed the computations and helped to draft the manuscript. All authors read and approved the final manuscript.

Conflicts of interest

The authors declare no conflicts of interest.

Acknowledgements

The authors are grateful for the financial support from the National Natural Science Foundation of China (No. 21871199 and 21933002). This work was also supported by the Collaborative Innovation Centre of Suzhou Nano Science and Technology (Nano-CIC), the Priority Academic Program Development of Jiangsu Higher Education Institutions (PAPD), and the ''111'' Project of the State Administration of Foreign Experts Affairs of China. C.-C. Wu acknowledges the support from the Ministry of Science and Technology of Taiwan (MOST 110-2221-E-002-104-MY3 and 111-2221-E-002-031-MY3).

References

1 U. Balijapalli, Y.-T. Lee, B. S. B. Karunathilaka, G. Tumen-Ulzii, M. Auffray, Y. Tsuchiya, H. Nakanotani and C. Adachi, *Angew. Chem., Int. Ed.*, 2021, **60**, 19364–19373.
2 (*a*) H. Uoyama, K. Goushi, K. Shizu, H. Nomura and C. Adachi, *Nature*, 2012, **492**, 234–238; (*b*) Y. Liu, J. Yang, Z. Mao, D. Ma, Y. Wang, J. Zhao, S.-J. Su and Z. Chi, *Adv. Opt. Mater.*, 2022, **11**, 2201695; (*c*) Y. X. Hu, J. Miao, T. Hua, Z. Huang, Y. Qi, Y. Zou, Y. Qiu, H. Xia, H. Liu, X. Cao and C. Yang, *Nat. Photonics*, 2022, **16**, 803–810; (*d*) X. Wu, B.-K. Su, D.-G. Chen, D. Liu, C.-C. Wu, Z.-X. Huang, T.-C. Lin, C.-H. Wu, M. Zhu, E. Y. Li, W.-Y. Hung, W. Zhu and P.-T. Chou, *Nat. Photonics*, 2021, **15**, 780–786; (*e*) D. Zhang, Y. Wada, Q. Wang, H. Dai, T. Fan, G. Meng, J. Wei, Y. Zhang, K. Suzuki, G. Li, L. Duan and H. Kaji, *Adv. Sci.*, 2022, **9**, 2106018.
3 A. Zampetti, A. Minotto and F. Cacialli, *Adv. Funct. Mater.*, 2019, **29**, 1807623.
4 Y. Xiao, H. Wang, Z. Xie, M. Shen, R. Huang, Y. Miao, G. Liu, T. Yu and W. Huang, *Chem. Sci.*, 2022, **13**, 8906–8923.
5 D.-H. Kim, A. D'Aléo, X.-K. Chen, A. D. S. Sandanayaka, D. Yao, L. Zhao, T. Komino, E. Zaborova, G. Canard, Y. Tsuchiya, E. Choi, J. W. Wu, F. Fages, J.-L. Brédas, J.-C. Ribierre and C. Adachi, *Nat. Photonics*, 2018, **12**, 98–104.
6 J. Kumsampao, C. Chaiwai, P. Chasing, T. Chawanpunyawat, S. Namuangruk, T. Sudyoadsuk and V. Promarak, *Chem. – Asian J.*, 2020, **15**, 3029–3036.
7 J. L. He, Y. Tang, K. Zhang, Y. Zhao, Y. C. Lin, C. K. Hsu, C. H. Chen, T. L. Chiu, J. H. Lee, C. K. Wang, C. C. Wu and J. Fan, *Mater. Horiz.*, 2022, **9**, 772–779.
8 J.-F. Cheng, F.-C. Kong, K. Zhang, J.-H. Cai, Y. Zhao, C.-K. Wang, J. Fan and L.-S. Liao, *Chem. Eng. J.*, 2022, **430**, 132822.
9 S. Wang, X. Yan, Z. Cheng, H. Zhang, Y. Liu and Y. Wang, *Angew. Chem., Int. Ed.*, 2015, **54**, 13068–13072.
10 Y. Yuan, Y. Hu, Y.-X. Zhang, J.-D. Lin, Y.-K. Wang, Z.-Q. Jiang, L.-S. Liao and S.-T. Lee, *Adv. Funct. Mater.*, 2017, **27**, 1700986.
11 J. Xue, Q. Liang, R. Wang, J. Hou, W. Li, Q. Peng, Z. Shuai and J. Qiao, *Adv. Mater.*, 2019, **31**, 1808242.
12 D. G. Congrave, B. H. Drummond, P. J. Conaghan, H. Francis, S. T. E. Jones, C. P. Grey, N. C. Greenham, D. Credgington and H. Bronstein, *J. Am. Chem. Soc.*, 2019, **141**, 18390–18394.
13 Q. Liang, J. Xu, J. Xue and J. Qiao, *Chem. Commun.*, 2020, **56**, 8988–8991.
14 Y. Yu, H. Xing, D. Liu, M. Zhao, H. H.-Y. Sung, I. D. Williams, J. W. Y. Lam, G. Xie, Z. Zhao and B. Z. Tang, *Angew. Chem., Int. Ed.*, 2022, **61**, e202204279.
15 Q. Li, J. Xu, S. Tan, Y. Dai, J. Xue and J. Qiao, *Org. Electron.*, 2022, **110**, 106645.
16 J.-F. Cheng, Z.-H. Pan, K. Zhang, Y. Zhao, C.-K. Wang, L. Ding, M.-K. Fung and J. Fan, *Chem. Eng. J.*, 2022, **430**, 132744.

Published on 30 kovo 2023. Downloaded on 2024-08-10 18:25:00.

17 Y. Yu, Y. Hu, S. Yang, W. Luo, Y. Yuan, C. Peng, J. Liu, A. Khan, Z. Jiang and L. Liao, *Angew. Chem., Int. Ed.*, 2020, **59**, 21578–21584.
18 T. Yang, B. Y. Liang, Z. Cheng, C. L. Li, G. Y. Lu and Y. Wang, *J. Phys. Chem. C*, 2019, **123**, 18585–18592.
19 H. Wang, B. Zhao, C. Qu, C. Duan, Z. Li, P. Ma, P. Chang, C. Han and H. Xu, *Chem. Eng. J.*, 2022, **436**, 135080.
20 Z. Cai, X. Wu, H. Liu, J. Guo, D. Yang, D. Ma, Z. Zhao and B. Z. Tang, *Angew. Chem., Int. Ed.*, 2021, **60**, 23635–23640.
21 T. Yang, J. Liang, Y. Cui, Z. Li, X. Peng, S.-J. Su, Y. Wang and C. Li, *Adv. Opt. Mater.*, 2022, **11**, 2201191.
22 (*a*) K. Wang, Y.-Z. Shi, C.-J. Zheng, W. Liu, K. Liang, X. Li, M. Zhang, H. Lin, S.-L. Tao, C.-S. Lee, X.-M. Ou and X.-H. Zhang, *ACS Appl. Mater. Interfaces*, 2018, **10**, 31515–31525; (*b*) K. Wang, C.-J. Zheng, W. Liu, K. Liang, Y.-Z. Shi, S.-L. Tao, C.-S. Lee, X.-M. Ou and X.-H. Zhang, *Adv. Mater.*, 2017, **29**, 1701476.
23 (*a*) J. Wang, J. Miao, C. Jiang, S. Luo, C. Yang and K. Li, *Adv. Opt. Mater.*, 2022, **10**, 2201071; (*b*) G. Zhao, D. Liu, P. Wang, X. Huang, H. Chen, Y. Zhang, D. Zhang, W. Jiang, Y. Sun and L. Duan, *Angew. Chem., Int. Ed.*, 2022, **61**, e202212861.
24 T. Tsuboi, H. Murayama, S.-J. Yeh and C.-T. Chen, *Opt. Mater.*, 2007, **29**, 1299–1304.
25 S.-P. Wang, Z. Cheng, X.-X. Song, X.-J. Yan, K.-Q. Ye, Y. Liu, G.-H. Yang and Y. Wang, *ACS Appl. Mater. Interfaces*, 2017, **9**, 9892–9901.
26 (*a*) W. Z. Yuan, X. Bin, G. Chen, Z. H. He, J. Liu, H. L. Ma, Q. Peng, B. W. Wei, Y. Y. Gong, Y. W. Lu, G. F. He and Y. M. Zhang, *Adv. Opt. Mater.*, 2017, **5**, 1700466; (*b*) Y. Y. Pan, J. Huang, Z. M. Wang, S. T. Zhang, D. W. Yu and Y. G. Ma, *RSC Adv.*, 2016, **6**, 108404.
27 (*a*) F. Tenopala-Carmona, O. S. Lee, E. Crovini, A. M. Neferu, C. Murawski, Y. Olivier, E. Zysman-Colman and M. C. Gather, *Adv. Mater.*, 2021, **33**, 2100677; (*b*) X. Zeng, Y.-H. Huang, S. Gong, X. Yin, W.-K. Lee, X. Xiao, Y. Zhang, W. Zeng, C.-H. Lu, C.-C. Lee, X.-Q. Dong, C. Zhong, C.-C. Wu and C. Yang, *Sci. China Mater.*, 2021, **64**, 920–930.
28 (*a*) X. Gong, C.-H. Lu, W.-K. Lee, P. Li, Y.-H. Huang, Z. Chen, L. Zhan, C.-C. Wu, S.-L. Gong and C.-L. Yang, *Chem. Eng. J.*, 2021, **405**, 126663; (*b*) B.-K. Wang, W.-K. Lee, K.-C. Lin, P.-J. Chen, Y.-H. Huang, S.-W. Wen, X. Zeng, F. Ni, S.-L. Gong, C.-L. Yang and C.-C. Wu, *Org. Electron.*, 2021, **89**, 106049.
29 J.-H. Tan, J.-M. Jin, W.-C. Chen, C. Cao, R. Wang, Z.-L. Zhu, Y. Huo and C.-S. Lee, *ACS Appl. Mater. Interfaces*, 2022, **14**, 53120–53128.
30 R. Huang, H. Chen, H. Liu, Z. Zhuang, J. Wang, M. Yu, D. Yang, D. Ma, Z. Zhao and B. Z. Tang, *Chem. Eng. J.*, 2022, **435**, 134934.
31 L. Peng, J. Lv, S. Xiao, Y. Huo, Y. Liu, D. Ma, S. Ying and S. Yan, *Chem. Eng. J.*, 2022, **450**, 138339.

This journal is © The Royal Society of Chemistry 2023